A Simulative Model of Dryline Motion

JOSEPH T. SCHAEFER

National Severe Storms Laboratory, NOAA, Norman, Okla. 73069

(Manuscript received 29 August 1973)

ABSTRACT

A dryline is a narrow zone, other than a classical polar front, across which a sharp horizontal surface moisture gradient occurs. It often exists and moves under synoptically quiescent conditions. One explanation of dryline motion is that it is caused by turbulent vertical mixing. A slab symmetric numerical model of the boundary layer is developed to test this hypothesis. This model, when applied to a typical dryline environment, produces dryline motions similar to those observed in the atmosphere. The model is applied to several real dryline cases, and a close correspondence between simulated and observed motions are found. It is concluded that vertical mixing is the primary cause of dryline motion.

1. Introduction

The dryline is a synoptic feature often associated with thunderstorm development over the southern plains (Rhea, 1966). This phenomenon is a narrow zone, other than a classical front, across which a sharp surface horizontal moisture gradient occurs. It approximately parallels the terrain contours and is often found over west Texas and Oklahoma during the spring and early summer. As the dryline moves eastward, it becomes progressively more diffuse and can seldom be followed east of 96W. Potentially cool, moist air is generally found east of the dryline trapped beneath a capping inversion or low-level stable layer, while in the region west of the dryline and above the inversion, potentially warm dry air exists (Carlson and Ludlam, 1968). The 9 gm kg^{-1} mixing ratio isohume has been found to approximately correspond to the dryline position (Schaefer, 1973a). The dryline surface has a characteristic step profile, being nearly vertical to 3000 or 4000 ft above its surface intercept. It then tilts rapidly to become a nearly horizontal surface eastward from the surface zone. In midafternoon, when the dryline exhibits the sharpest horizontal moisture discontinuities, the density differential across it is negligible (McGuire, 1962). Although the winds tend to veer across the dryline, the streamline confluence line does not coincide with the sharp moisture gradient (Matteson, 1969).

General dryline motion characteristics were discussed and a conceptual model of its driving mechanism was formulated in a previous paper (Schaefer, 1973a). Drylines which exist during quiet atmospheric conditions are usually typified by diurnal motion trends. They move eastward (away from the Rocky Mountains) during the day and westward at night. Dryline motion is characteristically non-uniform with different sections moving at different speeds. During the day, little correlation between wind speed and dryline velocity exists. On the average, horizontal advection by synoptic flow patterns account for only about 50% of the daytime motion. However, at night, the dryline behaves as if it were advected by the winds.

It was postulated that the major mechanism which causes dryline motion is vertical turbulent mixing between the two distinct air masses involved in the dryline environment. Mixing presumably affects dryline motion in the following manner. At dawn, boundary layer mixing is initiated as surface temperatures rise in response to insolation. West of the dryline, any nocturnal radiational inversion is rapidly destroyed and an approximately adiabatic lapse rate is established. Since the depth of the moist layer increases eastward, due to the general terrain slope, the heat required to erase the capping inversion increases in that direction causing a corresponding delay of inversion breakdown. Since the dryline lies approximately parallel to the surface elevation contour(s), the inversion height, and therefore the amount of heating required to break the inversion, is nearly uniform in that direction. When the required heat has been absorbed, the low-level moist air mixes with dry air aloft. A rapid drop in surface mixing ratio occurs and the dryline "leaps" eastward to a position where no appreciable vertical mixing between air masses has occurred.

Toward early evening, the low-level temperatures start their diurnal fall. Since dry air cools more rapidly than moist air, a radiational inversion which inhibits vertical mixing of momentum and heat rapidly forms west of the dryline resulting in a decreasing and backing of the surface flow in the dry air. The less rapid cooling in the moist air allows nearly steady flow to be maintained east of the dryline. The resulting net easterly wind component advects the dryline westward.

2. The physical model

A model of the dryline environment was developed to verify the hypothesis that vertical turbulent mixing is the primary cause of dryline motion. The meteorological parameters parallel to the dryline are approximately homogeneous so an assumption of slab-symmetry similar to that used by Estoque and Bhumralker (1968) can be made. This assumption implies that all atmospheric variables except pressure are constant in the vertical planes parallel to the dryline and that the pressure gradient component in that direction is constant.

Since the moist air intersects the earth's surface and is generally less than 2 km deep, the dryline is a low-level phenomenon. Because it often moves under synoptically quiescent conditions, a model of the planetary boundary layer should suffice to depict the dryline and the physical processes which control its motion.

In such a model, the ratio of the vertical scale to the horizontal one is very small and the hydrostatic approximation is valid (Milne-Thomson, 1960). Boundary layer shallowness also allows the neglect of density changes (Ogura and Phillips, 1962). Turbulent processes are parameterized using eddy coefficient relationships. While this parameterization precludes countergradient fluxes, it is used instead of higher order closure techniques (e.g., Deardorff, 1972) because such methods require many arbitrary constants which have not yet been empirically determined.

If it is assumed that the atmosphere is cloudless and that radiative heating takes place only at the earth-atmosphere interface, the first law of thermodynamics states that eddy conduction is the only process which can change a parcel's potential temperature. Also, since there are no appreciable moisture sources or sinks in such an atmosphere, water vapor is assumed to be conserved.

3. The computational model

The computational model used in this study employs a two-dimensional x-z system on a polar stereographic projection, where x is the coordinate normal to the dryline and z the elevation above surface. This vertical coordinate allows for varying elevation (E) of the terrain above sea level. Terms associated with the variability of the map factor m, defined by

$$m=(1+\sin 60)/(1+\sin\varphi), \tag{1}$$

where φ is the latitude, are neglected. The horizontal equations of motion in this system are

$$\frac{\partial u}{\partial t}+mu\frac{\partial u}{\partial x}+W\frac{\partial u}{\partial z}=f(v-v_g)+\frac{\partial}{\partial z}\left(K_M\frac{\partial u}{\partial z}\right), \tag{2}$$

$$\frac{\partial v}{\partial t}+mu\frac{\partial v}{\partial x}+W\frac{\partial v}{\partial z}=f(u_g-u)+\frac{\partial}{\partial z}\left(K_M\frac{\partial v}{\partial z}\right), \tag{3}$$

where

$$W=w-mu\left.\frac{\partial E}{\partial x}\right|_z, \tag{4}$$

$$u_g=-m\theta\Big/\left(f\frac{\partial \pi}{\partial y}\right), \tag{5}$$

$$v_g=m\theta\Big/\left(f\left.\frac{\partial \pi}{\partial x}\right|_s\right)+mg\Big/\left(f\left.\frac{\partial E}{\partial x}\right|_z\right), \tag{6}$$

$$\pi=c_p(p/p_0)^{R/c_p}. \tag{7}$$

The other symbols are defined as follows:

c_p	specific heat of dry air at constant pressure
E	surface elevation above sea level
f	Coriolis parameter
g	acceleration of gravity
K_M	eddy viscosity coefficient
p	pressure
p_0	reference pressure (1000 mb)
R	specific gas constant for dry air
t	time
u	component of motion normal to the dryline
v	component of motion parallel to the dryline
w	vertical component of motion
θ	potential temperature

As mentioned before, the third component equation of motion is approximated by the hydrostatic equation

$$\frac{\partial \pi}{\partial z}=-g\theta^{-1}. \tag{8}$$

The continuity equation is

$$m\frac{\partial u}{\partial x}+\frac{\partial W}{\partial z}=0. \tag{9}$$

The thermodynamic energy equation and the conservation for water vapor are given by

$$\frac{\partial \theta}{\partial t}+u\frac{\partial \theta}{\partial x}+W\frac{\partial \theta}{\tau z}=\frac{\partial}{\partial z}\left(K_H\frac{\partial \theta}{\partial z}\right), \tag{10}$$

$$\frac{\partial Q}{\partial t}+u\frac{\partial Q}{\partial x}+W\frac{\partial Q}{\partial z}=\frac{\partial}{\partial z}\left(K_V\frac{\partial Q}{\partial z}\right). \tag{11}$$

In the above, K_H denotes eddy thermal diffusivity, K_V eddy diffusivity for water vapor, and Q mixing ratio.

If the eddy coefficients are known, Eqs. (2), (3), (8), (9), (10) and (11), together with proper initial and boundary conditions, form a complete set of governing equations. Among them four are prognostic for u, v, θ and Q, while two are diagnostic for π and w.

4. Determination of the eddy coefficients for momentum, heat and moisture

Since the purpose of this model is to diagnose the physical processes pertinent to dryline motion, not to forecast or portray the anemometer-level wind field, the theoretically complicated parameterizations needed to prescribe physical variables in the contact layer (Tennekes and Lumley, 1972) are not attempted. For simplicity, a no-slip condition at the surface is enforced and the surface temperature is assumed as a function of time. The eddy coefficients for momentum, heat and moisture in the lowest layer of the model are evaluated using equations given by Estoque (1962).

Two distinct turbulent mixing regimes are allowed. Free convection is associated with thermals arising from surface heating, and forced convection with mixing brought about by mechanical turbulence in a thermodynamically stable or nearly stable atmosphere. The transition between these two categories occurs at a gradient Richardson number

$$\mathrm{Ri}=\frac{g}{\theta}\frac{\partial\theta/\partial z}{(\partial s/\partial z)^2} \tag{12}$$

(where s is the wind speed) of -0.03 (see Estoque, 1963; Pandolfo, 1966; Gerrity, 1967). For free convection ($\mathrm{Ri}<-0.03$), the eddy thermal diffusivity, developed using similarity theory (Priestley, 1959), is formulated as

$$K_H=\lambda z^2\left|\frac{g}{\theta}\frac{\partial\theta}{\partial z}\right|^{\frac{1}{2}}, \tag{13}$$

where λ is an arbitrary constant. For forced convection ($\mathrm{Ri}>-0.03$), the eddy viscosity assumes the form as given by Pandolfo *et al.* (1963), i.e.,

$$\begin{aligned} K_M&=[kz(1-\beta\,\mathrm{Ri})]^2\left|\frac{\partial s}{\partial z}\right|, \text{ if } 1-\beta\,\mathrm{Ri}>0,\\ &=1, \text{ if } 1-\beta\,\mathrm{Ri}<0, \end{aligned} \tag{14}$$

where k is the von Kármán constant and β another arbitrary constant. A functional relationship between λ and β has been determined by Gerrity (1967), and his values of 1.2 and 2.0, respectively, are used here.

To solve the basic equations, the relationship between the eddy thermal diffusivity and the eddy viscosity must be known. The order of magnitude approximation that the eddy Prandtl number (K_M/K_H) is unity is often used. However, for the atmospheric boundary layer this is not very precise. The observational fact that the moisture discontinuity does not occur at the wind shift line in the dryline environment substantiates the assertion that these two quantities are not equal. In Gerrity's (1967) boundary layer model, the ratio K_H/K_M (inverse eddy Prandtl number) is given the value of unity in the forced convection regime, but for free convection it is arbitrarily increased to 1.3. Businger (1966), through an examination of the second moment equation of turbulence, determined the dependence of this ratio upon stability. His equation is derived for mid-ranges of stability. In both very stable and very unstable conditions, the ratio becomes constant. The value under strongly stable conditions is 0.25 while for highly unstable conditions it is 2.0 (Businger *et al.*, 1971).

The ratio is given by the Businger-Dyer relationship as

$$K_H/K_M=[1-18(z/L)]^{\frac{1}{4}}, \tag{15}$$

where L is the Obukhov length. For unstable conditions ($\mathrm{Ri}<0$), the ratio K_H/K_M is equal to the Richardson number (Swinbank, 1968), and for stable conditions the relationship

$$(z/L)=(K_H/K_M)\left(\frac{\mathrm{Ri}}{1-7\,\mathrm{Ri}}\right), \tag{16}$$

holds (McVehil, 1964). Thus, from the Richardson number, the ratio of the eddy coefficients can be obtained either by direct application of (15) for unstable conditions or by using Ferrari's theorem (James and James, 1959) to solve for the real positive root of the quartic equation obtained by combining (15) and (16).

The computed value of the vertical eddy viscosity coefficient is limited to ranges between 1 and 100 m^2 sec^{-1} so that it agrees with empirical determinations (Wu, 1965). If either bound is exceeded, the coefficient is set equal to that bound. The eddy diffusivity for water vapor is set equal to the eddy thermal diffusivity since the second-moment equations for both potential temperature and mixing ratio are independent of pressure and are of basically the same form (Swinbank and Dyer, 1967).

The variation of the eddy coefficients with height is determined by vertical extrapolation of the low-level value by means of the O'Brien (1970) profile. This is necessary because the formulas for eddy coefficient determinations are valid only for the lowest layer of the atmosphere. If the top of the boundary layer is designated as level A and the top of the contact layer [where (13) and (14) are valid] is level B, the vertical distribution of the eddy coefficient is given by

$$K(z)=\left[\frac{(z-z_A)}{(z_A-z_B)}\right]^2 \times\left\{K_B+(z-z_B)\left[\left.\frac{\partial K}{\partial z}\right|_B+\frac{2K_B}{(z_A-z_B)}\right]\right\}, \tag{17}$$

where K_B, the value of K at level B, is determined by using (13) through (16), and its derivative is obtained by assuming a constant flux across level B.

5. Application of the equations to the dryline environment

To show the motion of the dryline, the modeled environment must have a horizontal dimension large enough to include regions on both sides of the dryline which are not affected by the motion. Since the dryline often moves more than 500 km eastward during the daytime hours, a horizontal dimension of 1000 km (at 60N) was chosen. Observational sparcity in the region of most frequent dryline occurrence denies the specification of meteorological parameters on a scale smaller than 100 km. Accordingly, the horizontal dimension was divided into 10 equally spaced increments. Because the dryline inversion lies 2–3 km above the surface, the depth of the model atmosphere was set at 3.8 km above the surface with 20 vertical grid points separated by 200 m.

In the finite-difference form of the equations, time derivatives were approximated by Euler forward differences. Advection terms in prognostic equations were computed using upstream differences. Centered differences were employed for eddy flux convergence, vertical velocity and pressure computation. This finite-difference scheme is classically used in multi-dimensional boundary layer models (Estoque, 1962; Gerrity, 1967; etc). While upstream differencing introduces a computational viscosity, for this model's large spatial increment it produces a more accurate solution than centered space differencing which smooths fine-scale features (Marchuk, 1964).

In the linear approximation of the modelling equations, the time increment Δt must be chosen to satisfy both the Courant-Friedrichs-Lewy advective stability criterion,

$$\Delta t < \Delta x/u, \tag{18}$$

where Δx is the horizontal space increment, and the diffusive stability criterion (Ames, 1965)

$$\Delta t < \Delta z^2/2K, \tag{19}$$

where Δz is the vertical space increment. Since the model is nonlinear, a time step of 90 sec (much less than required by the above linear criteria) was used.

6. Boundary and initial conditions

The numerical integration of the modelling equations requires boundary conditions that are not only consistent with the mathematical equations and the observed physical conditions of the dryline environment, but also with the finite-difference analogues used. In the prognostic equations (2), (3), (10) and (11), the upstream lateral boundary condition is

$$\left.\frac{\partial A}{\partial x}\right|_{s_{\text{upwind}}} = 0, \tag{20}$$

where A is either u, v, θ or Q. This condition provides

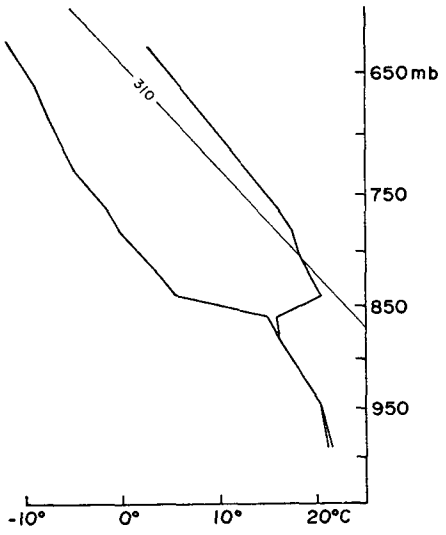

FIG. 1. A "typical" sounding east of the dryline.

homogeneity of meteorological variables outside of the region affected by the dryline. In the diagnostic equations for the pressure gradient (geostrophic wind, v_g) and vertical velocity, the centered difference along the lateral walls is replaced by a one-sided difference.

At the top boundary ($z=3.8$ km), due to the synoptically quiescent atmosphere usually coexistent with the dryline, the flow is assumed geostrophic, and potential temperature, mixing ratio and pressure are assumed constant in time. At the earth's surface, a no-slip boundary is postulated. No turbulent moisture flux through the surface is allowed. Since this is a diagnostic model, the time dependence of the surface temperature is specified.

Initial data for the model were derived from a sounding taken well east of the dryline (Fig. 1), and surface potential temperature values across the dryline. These potential temperatures, when combined with an estimated geostrophic wind field, are sufficient to solve

$$\frac{\partial \theta}{\partial x} = -\frac{f}{g}\left[\theta\frac{\partial v_g}{\partial z} - \left(v_g - \frac{g}{f}\frac{\partial E}{\partial x}\right)\right]\frac{\partial \theta}{\partial z} \tag{21}$$

for a potential temperature field. Eq. (21) arises from combining the geostrophic wind definition with the hydrostatic equation by cross differentiation. This "first guess" potential temperature field is filtered to eliminate superadiabatic layers and obtain an initial potential temperature field. The hydrostatic equation then provides the pressure field which is used to obtain an updated geostrophic wind field.

The initial mixing ratio distribution is formulated as a function of potential temperature determined from the soundings. The wind field is determined by solving the generalized Ekman equation (Schaefer, 1973b), with an eddy coefficient distribution given by (17) with a minimum constant flux eddy viscosity (1 m^2

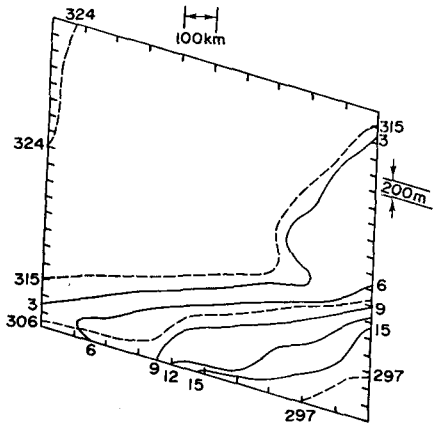

FIG. 2. Potential temperature (°K) and mixing ratio (gm kg^{-1}) fields used as initial conditions for case A: potential temperature (dashed lines), mixing ratio (solid lines).

sec^{-1}) and having a vertical derivative of 0.5 m sec^{-1}. The fields obtained are consistent with both model equations and observations in the vicinity of drylines.

7. Application of the model

The model is intended to indicate whether vertical turbulent mixing can be the primary cause of dryline motion. The equations are integrated using initial conditions which represent the typical quiescent dryline environment. Simplified versions of the model with advective and eddy mixing terms sequentially neglected are also used. Calculations are made for several different initial conditions and for different surface temperature distributions. Finally the model is tested on actual dryline data to see how accurately it simulates the real atmosphere.

One problem with this two-dimensional representation is the assumed constant pressure gradient parallel to the dryline. This assumption results in a constant principal forcing function for the normal component of motion. Because of this, the correlation between model dryline motion and observed dryline motion is expected to be degraded.

8. A typical dryline situation: Westerly geostrophic wind

For the first series of tests, the integration domain was oriented from west to east with the dryline positioned between grid points 4 and 5. A homogeneous terrain with a constant slope (10^{-3} from west to east), approximately conforming to the mean slope of the Texas-Oklahoma region, was used. On the eastern edge of the domain, a strong inversion and mixing ratio decrease between 1.2 and 1.4 km above the surface (Fig. 2) was assumed. The initial data were assumed to apply to 0600 local time, so a radiational inversion was present west of the dryline. The specified surface potential temperature increases linearly by 10C from east to west over the 1000 km domain. Initial potential temperature and mixing ratio distributions are shown in Fig. 2. These conditions are similar to those of a "typical" dryline.

The westerly component of the geostrophic wind is assumed to be 10 m sec^{-1}. A sinusoidal temporal surface temperature variation is assumed with the maximum occurring about 10 hr into the experiment. The amplitude of the temperature curve at the western edge is set at 10C, and it varies in space in such a manner that the surface virtual temperature is approximately constant over the domain at the time of maximum temperature. For future reference these conditions are labeled as Case A.

A plot of the model-produced temporal surface mixing ratio variation is given in Fig. 3. During the first 2 hr of simulation, little change in moisture distribution west of the dryline occurred, but a decrease in the extremely high values (>15 gm kg^{-1}) well to the east may be noted. As heating continued, surface mixing ratios decreased dramatically. The decrease was systematic so that the dryline moved rapidly eastward toward lower elevations. Between 6 and 7 hr from the start (1200 through 1300) the 9 gm kg^{-1} isopleth moved over 100 km eastward. As the surface temperatures approached a maximum at 1600 dryline motion slowed and almost completely stalled for the remaining 14 hr of the integration. As expected, the nocturnal return of the dryline did not appear in this example, because the strong westerly component of the geostrophic wind specified over the domain prevented easterly winds from developing in the moist air.

The model was then run with the same initial conditions but with the advection terms in (2), (3), (10) and (11) set equal to zero. The temporal variation of the surface mixing ratio for this case should be essentially as before if mixing is the dominant mechanism in dry line motion. Again, in the first 2 hr of the inte-

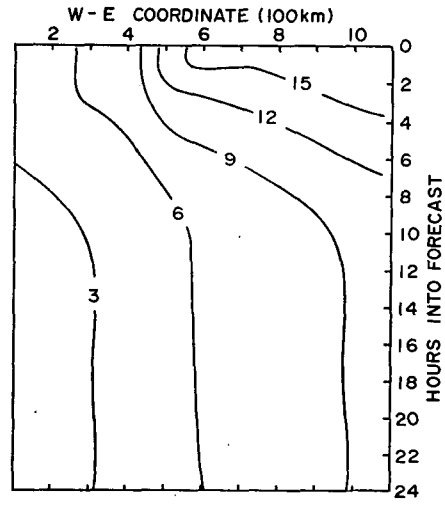

FIG. 3. Mixing ratio (gm kg^{-1}) variation with time for case A.

gration, the only appreciable change in the moisture field occurred in the extremely moist air on the east end of the grid (Fig. 4). During the remainder of the surface heating period, the pattern of drying progressed as before. As the heating rate decreases, the dryline motion stops more rapidly than for Case A, but even after 24 hr the dryline is located within 60 km of the Case A position. Thus, after 24 hr, the dryline moved 500 km without advection and 560 km with it. For this case wind-forced movement accounts for only 12% of the total dryline displacement.

To investigate the relative importance of advection when the dryline is moving rapidly, the eddy terms were neglected and only advection allowed to act. The dryline moved very little (Fig. 5) during the first 12 hr. Afterward, there was an acceleration, but even then the velocity was much less than the modelled daytime wind speeds with active mixing. This nocturnal increase in the "no eddy" process case is caused by progression of the winds around the inertial circle to a supergeostrophic velocity. Without vertical mixing retarding the inertial tendency, faster nocturnal wind speeds occur than in the other examples where a forced mixing was present even under thermodynamically stable conditions.

For the final example using this set of initial conditions, the model was run with one-half the amplitude of the diurnal temperature wave used in Case A. With this reduced heating, the dryline moved only about 100 km during the 10 hr of rising surface temperatures (Fig. 6) but this is still 80% more displacement than occurred during the same time span in the eddy-free example (Fig. 5).

9. A typical dryline situation: Easterly geostrophic wind

In the next series of integrations, all parameters are the same as in Case A except that the sign of the westerly component of the geostrophic wind is changed. Thus the forcing function in the u-component equation of motion has a value of -10 m sec^{-1}. The surface mixing ratio field produced by the model is given in Fig. 7. Eastward dryline motion was considerably less than when the geostrophic wind was westerly (Fig. 3), but it still moves 350 km during the time of surface heating. After the heating stops, the dryline drifts about 50 km back toward the west with the winds. This example demonstrates that the combination of vertical mixing and horizontal advection can yield the characteristic diurnal motion of the dryline.

The potency of vertical mixing as a cause of dryline motion is seen by a comparison of these results to those obtained when horizontal advection alone is allowed to act (Fig. 8). With strong easterly forcing, the dryline moves continually westward. When advection is

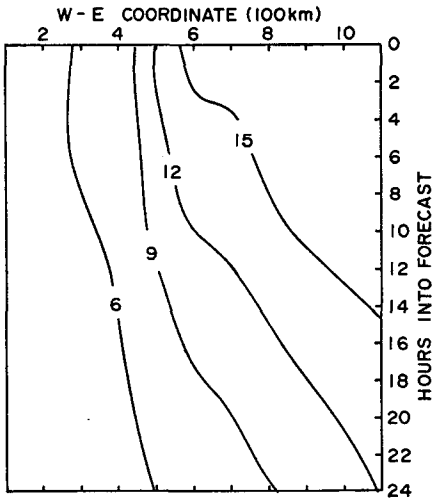

FIG. 5. Mixing ratio (gm kg^{-1}) variation with time for case A but with no mixing allowed.

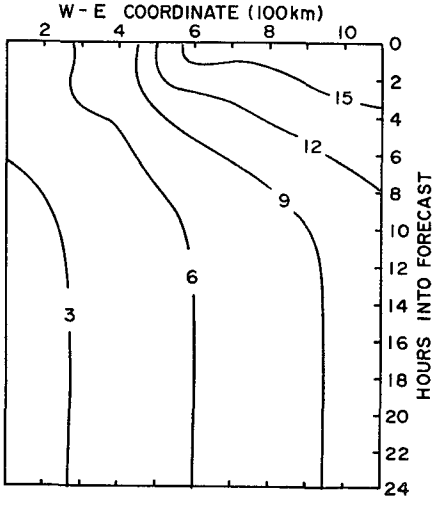

FIG. 4. Mixing ratio (gm kg^{-1}) variation with time for case A but with no advection allowed.

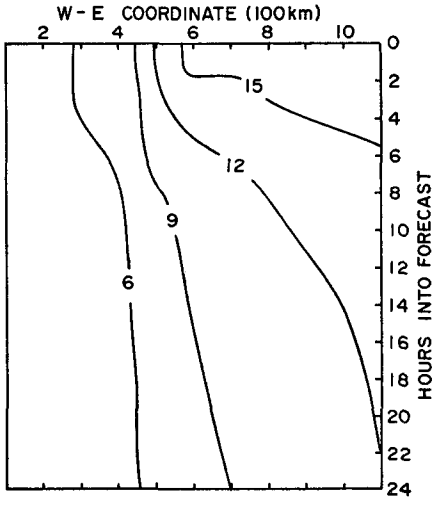

FIG. 6. Mixing ratio (gm kg^{-1}) variation with time for case A but with surface heating reduced 50%.

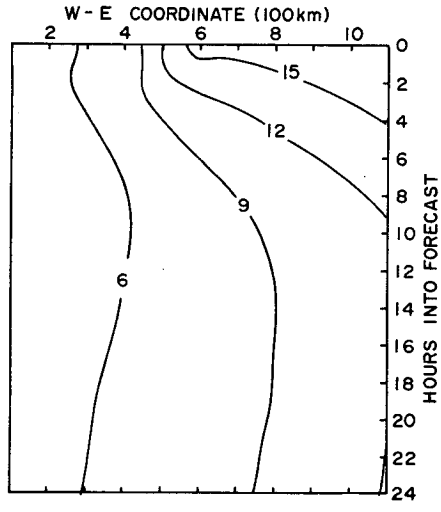

FIG. 7. Mixing ratio (gm kg^{-1}) variation with time for "typical" conditions but with an easterly geostrophic component.

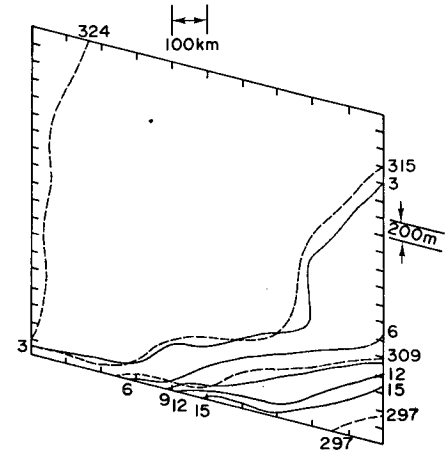

FIG. 9. Potential temperature (°K) and mixing ratio (gm kg^{-1}) fields used as initial conditions with the inversion lowered 400 m from its case A position: potential temperature (dashed lines), mixing ratio (solid lines).

neglected and mixing is allowed, the model output is substantially the same as was the case with the westerly geostrophic wind (Fig. 5). These experiments indicate that mixing produces a rapid daytime eastward dryline movement even against a strong easterly wind.

10. The effect of the inversion height

A major premise in dryline motion theory is that the dryline velocity decreases with increasing inversion height. To test this, the conditions of Case A were modified slightly. First, the height of the inversion was decreased by 400 m. The initial potential temperature and mixing ratio fields (Fig. 9) show that while the inversion is lower, the packing of the isentropes makes it stronger than in Case A. As expected, the dryline moved much faster (Fig. 10) than in the case with the higher inversion (Fig. 3). It is interesting that, while the initial dryline motion was delayed due to the increased strength of the lowered inversion, once motion began the dryline moved 100 km further eastward during the hours of surface heating than for Case A.

With the inversion raised 400 m above the level in Case A (Fig. 11), the dryline moves about 100 km less (Fig. 12) than it did in Case A. The initial eastward displacement of the 6 gm kg^{-1} isohume is caused by a negative hydrolapse (moisture increasing with height) west of the dryline in the initial mixing ratio field.

11. Simulation of actual dryline motion

The preceding numerical experiments indicate that vertical mixing plus advection is capable of yielding

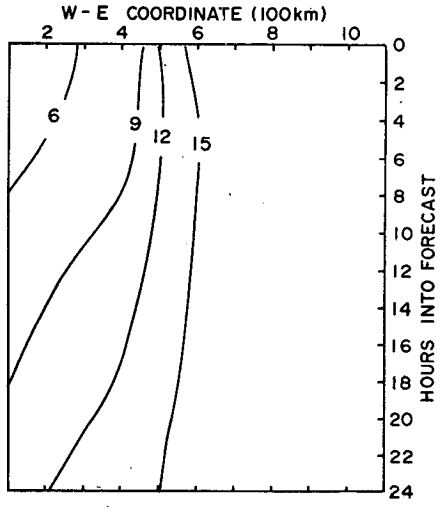

FIG. 8. Mixing ratio (gm kg^{-1}) variation with time for "typical" conditions but with an easterly geostrophic component and no mixing allowed.

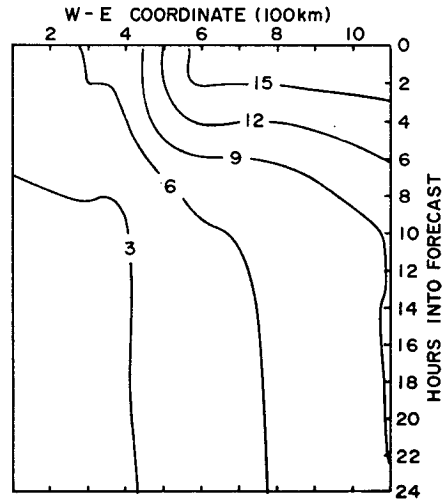

FIG. 10. Mixing ratio (gm kg^{-1}) variation with time for the inversion lowered 400 m from its case A position.

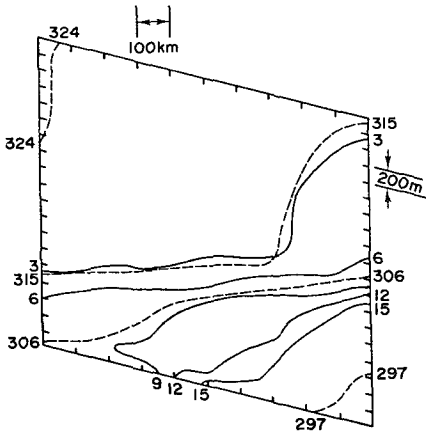

FIG. 11. Potential temperature (°K) and mixing ratio (gm kg ^{1}) fields used as initial conditions with the inversion raised 400 m from its Case A position: potential temperature (dashed lines), mixing ratio (solid lines).

dryline displacements similar to those observed. In order to see how well the simple two-dimensional model depicts actual dryline motion, data from three different dryline cases were used to initialize the model. The integration domain runs from Fort Worth on the east to central New Mexico on the west. This orientation places the Fort Worth (FTW) radiosonde data along the right edge of the grid.

The first such case simulated was the 22 May 1966 dryline. The initial conditions were obtained from a 1200 GMT surface analysis and the FTW sounding. The diurnal temperature curve amplitude is varied linearly across the domain from a maximum value of 7C at the western edge to 4.5C in the extreme east. These values agree with observed temperatures in the modelled region.

The results of the first 12 hr of simulation are shown

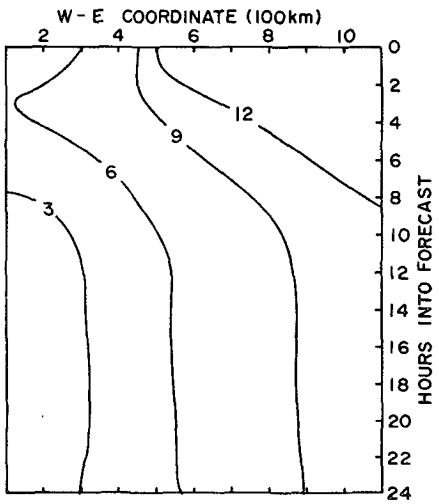

FIG. 12. Mixing ratio (gm kg^{-1}) variation with time for the inversion raised 400 m from its case A position.

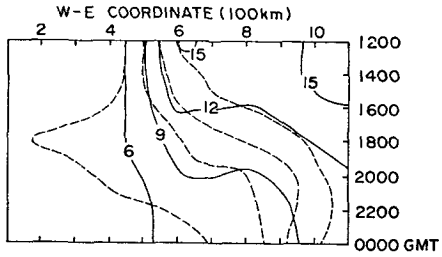

FIG. 13. Mixing ratio (gm kg^{-1}) variation with time on 22 May 1966 as simulated by the model and as observed: solid lines, simulation; dashed lines, observed.

in Fig. 13. They are very similar to the previous experiments. The "dryline" (9 gm kg^{-1} isohume) remains approximately stationary until sufficient heating occurs to break the low-level inversion. Then the dryline rapidly moves eastward at 1900 and 2000 GMT. The last 12 hr of the integration are not shown because the model requirements of a constant westerly geostrophic component obviates realistic representation of nocturnal dryline motion. Superimposed on Fig. 13 is the observed mixing ratio pattern. The dryline position shows good agreement between the numerical experiment and the observations, with approximately 75% of the total dryline displacement accounted for by the model. The discrepancy between simulation and observations west of the dryline is caused by the artificial horizontal diffusion inherent in the upstream differencing scheme combined with the restrictive requirement of a constant westerly geostrophic wind component. This latter constraint denies any prolonged moisture influx through the eastern boundary.

For the second test, the dryline of 11 April 1966 was simulated (Fig. 14). The amplitude of the diurnal temperature curve was varied from 14C in the west to 4C in the east. The environment on this day was not truly quiescent since a closed circulation was present over southwestern Oklahoma and northern Texas. Because of this synoptic activity, the model yielded a poor moisture field representation west of the dryline. However, even under these conditions, the movement of the dryline is quite accurately portrayed. Both the timing of the initial acceleration and the total dryline displacement demonstrate the validity of the model assumptions and assertions.

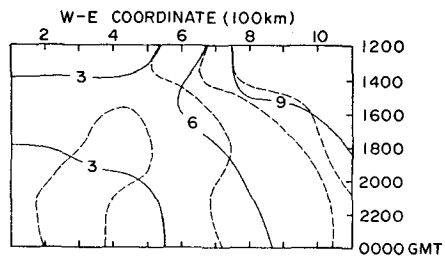

FIG. 14. As in Fig. 13 except for 11 April 1966.

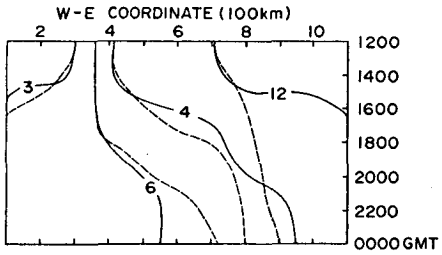

FIG. 15. As in Fig. 13 except for 5 June 1966.

The final test was made with the 5 June 1966 dryline. For this date the temperature curve amplitude was varied from 10C to 5C across the domain. This simulation (Fig. 15) shows remarkable agreement with the observations. As in the first example, the only major disagreement between numerical results and actual moisture distribution is east of the dryline.

12. Conclusion

The postulate that vertical turbulent mixing is the major contribution to dryline motion has been tested by means of a slab-symmetric boundary layer model. Numerical experiments on the "typical" dryline environment demonstrate that mixing produces realistic daytime dryline motion. The model qualitatively shows that as vertical mixing increases the dryline moves more rapidly. It also shows that vertical mixing is even capable of moving the dryline against adverse wind.

When the model is applied to actual data, the moist air east of the dryline shows spurious drying caused by the restrictions of its two-dimensionality. However, the simulated dryline motion (9 gm kg^{-1} isohume) exhibits very close agreement with observed phenomena. Thus, the model verifies that mixing is not only capable of producing dryline motion similar to that observed, but also yields a quantitatively accurate representation of dryline motion.

Acknowledgments. This paper is an extract of a Ph.D. dissertation from Saint Louis University. I gratefully acknowledge the assistance of Dr. Edwin Kessler, Director of the National Severe Storms Laboratory, whose ideas and interest in the dryline stimulated this work. I am also indebted to Drs. Donald E. Martin, Yeong-jer Lin and G. V. Rao of Saint Louis University who devoted considerable time and effort to this project since it forms an integral part of the research being done under National Science Foundation Grant GA 26029 to that University.

REFERENCES

Ames, W. F., 1965: *Nonlinear Partial Differential Equations in Engineering*. New York, Academic Press, 511 pp.

Businger, J. A., 1966: Transfer of momentum and heat in the planetary boundary layer. *Proc. Symp. Arctic Heat Budget and Atmospheric Circulation*, The Rand Corporation, Santa Monica, Calif., 305–322.

——, J. C. Wyngaard, Y. Isuma and E. F. Bradley, 1971: Flux profile relationships in the atmospheric surface layer. *J. Atmos. Sci.*, **25**, 1021–1033.

Carlson, T. N., and F. H. Ludlam, 1968: Conditions for the occurrence of severe local storms. *Tellus*, **20**, 203–226.

Deardorff, J. W., 1972: Numerical integration of the neutral and unstable planetary boundary layers. *J. Atmos. Sci.*, **29**, 91–115.

Estoque, M. A., 1962: The sea breeze as a function of the prevailing synoptic situation. *J. Atmos. Sci.*, **19**, 244–250.

——, 1963: A numerical model of the atmospheric boundary layer. *J. Geophys. Res.*, **68**, 1103–1113.

——, and C. M. Bhumralker, 1968: Theoretical studies of the atmospheric boundary layer. Final Report, Contract ECOM-6702-F, U. S. Army Electronics Command, Atmos. Sci. Lab., Fort Huachuca, Ariz., 46 pp.

Gerrity, J. P., 1967: A physical-numerical model for the prediction of synoptic-scale low cloudiness. *Mon. Wea. Rev.*, **95**, 261–268.

James, G. J., and R. C. James, 1959: *Mathematics Dictionary*. Princeton, N. J., Van Nostrand, 546 pp.

Marchuk, G. I., 1964: A new approach to the numerical solution of differential equations of atmospheric processes. *Theory of the General Circulation*, WMO Tech. Note No. 66, Geneva, 212–226.

Matteson, G. T., 1969: The West Texas dry front of June 1967. M.S. thesis, University of Oklahoma, Norman.

McGuire, E. L., 1962: The vertical structure of three dry lines as revealed by aircraft traverses. National Severe Storms Project Report No. 7, Norman, Okla., 10 pp.

McVehil, G. E., 1964: Wind and temperature profiles near the ground in stable stratification. *Quart. J. Roy. Meteor. Soc.*, **90**, 136–147.

Milne-Thomson, L. M., 1960: *Theoretical Hydrodynamics*, 4th ed. New York, MacMillian, 660 pp.

O'Brien, J. J., 1970: A note on the vertical structure of the eddy exchange coefficient in the planetary boundary layer. *J. Atmos. Sci.*, **27**, 1213–1215.

Ogura, Y., and N. A. Phillips, 1962: Scale analysis of deep and shallow convection in the atmosphere. *J. Atmos. Sci.*, **19**, 173–179.

Pandolfo, J. P., D. S. Cooley, and E. A. Newburg, 1963: Preliminary investigations of numerical models for short-period prediction of wind, temperature and moisture in the atmospheric boundary layer. Final Report 7047, Contract CWB-10368, Travelers Research Center, Hartford, Conn., 88 pp.

Pandolfo, J. P., 1966: Wind and temperature profiles for constant flux boundary layers in lapse conditions with a variable eddy conductivity to eddy viscosity ratio. *J. Atmos. Sci.*, **23**, 495–502.

Priestley, C. H. B., 1959: *Turbulent Transfer in the Lower Atmosphere*. The University of Chicago Press, 130 pp.

Rhea, J. O., 1966: A study of thunderstorm formation along dry lines. *J. Appl. Meteor.*, **5**, 58–63.

Schaefer, J. T., 1973a: The motion of the dryline. *Preprints Eighth Severe Storms Conf.*, Denver, Colo., Amer. Meteor. Soc., 104–107.

——, 1973b: On the solution of the generalized Ekman equation. *Mon. Wea. Rev.* (in press).

Swinbank, W. C., 1968: A comparison between predictions of dimensional analysis for the constant flux layer and observations in unstable conditions. *Quart. Roy. Meteor. Soc.*, **96**, 67–90.

——, and A. J. Dyer, 1967: An experimental study in micrometeorology. *Quart. J. Roy. Meteor. Soc.*, **93**, 494–500.

Tennekes, H., and J. L. Lumley, 1972: *A First Course in Turbulence*. The MIT Press, 300 pp.

Wu, S. S., 1965: A study of heat transfer coefficients in the lowest 400 meters of the atmosphere. *J. Geophys. Res.*, **70**, 1801–1807.